This is an open access article published under an ACS AuthorChoice License, which permits copying and redistribution of the article or any adaptations for non-commercial purposes.

ACS AuthorChoice

NANO LETTERS

Mini Review

Cite This: Nano Lett. XXXX, XXX, XXX−XXX

pubs.acs.org/NanoLett

The Role of Polarity in Nonplanar Semiconductor Nanostructures

María de la Mata,[*,†,◆] Reza R. Zamani,[‡] Sara Martí-Sánchez,[†] Martin Eickhoff,[§] Qihua Xiong,[∥] Anna Fontcuberta i Morral,[⊥,#] Philippe Caroff,[∇] and Jordi Arbiol[*,†,○]

[†]Catalan Institute of Nanoscience and Nanotechnology (ICN2), CSIC and BIST, Campus UAB, Bellaterra, 08193 Barcelona, Catalonia, Spain

[‡]Interdisciplinary Center for Electron Microscopy, CIME, École Polytechnique Fédérale de Lausanne (EPFL), 1015 Lausanne, Switzerland

[§]Institute of Solid State Physics, University of Bremen, 28359 Bremen, Germany

[∥]School of Physical and Mathematical Sciences, Nanyang Technological University, 637371 Singapore

[⊥]Laboratory of Semiconductor Materials, Institute of Materials, School of Engineering and [#]Institute of Physics, School of Basic Sciences, École Polytechnique Fédérale de Lausanne (EPFL), 1015 Lausanne, Switzerland

[∇]Microsoft Quantum Lab Delft, Delft University of Technology, 2600 GA Delft, The Netherlands

[○]ICREA, Pg. Lluís Companys 23, 08010 Barcelona, Catalonia, Spain

Supporting Information

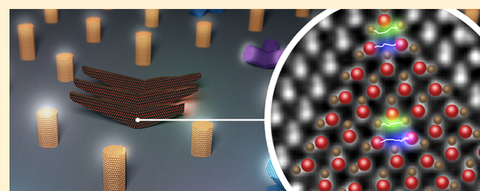

ABSTRACT: The lack of mirror symmetry in binary semiconductor compounds turns them into polar materials, where two opposite orientations of the same crystallographic direction are possible. Interestingly, their physical properties (e.g., electronic or photonic) and morphological features (e.g., shape, growth direction, and so forth) also strongly depend on the polarity. It has been observed that nanoscale materials tend to grow with a specific polarity, which can eventually be reversed for very specific growth conditions. In addition, polar-directed growth affects the defect density and topology and might induce eventually the formation of undesirable polarity inversion domains in the nanostructure, which in turn will affect the photonic and electronic final device performance. Here, we present a review on the polarity-driven growth mechanism at the nanoscale, combining our latest investigation with an overview of the available literature highlighting suitable future possibilities of polarity engineering of semiconductor nanostructures. The present study has been extended over a wide range of semiconductor compounds, covering the most commonly synthesized III−V (GaN, GaP, GaAs, GaSb, InN, InP, InAs, InSb) and II−VI (ZnO, ZnTe, CdS, CdSe, CdTe) nanowires and other free-standing nanostructures (tripods, tetrapods, belts, and membranes). This systematic study allowed us to explore the parameters that may induce polarity-dependent and polarity-driven growth mechanisms, as well as the polarity-related consequences on the physical properties of the nanostructures.

KEYWORDS: *Polarity, semiconductor, III−V, II−VI, growth mechanisms, nanostructures, nanowires*

The charge transfer between constituents in ionic crystals leads to distortions of their coordination geometry; namely, tetrahedral, which translates into two-dimensional (2D) projected atomic couples where the ions are oppositely charged. As a consequence, internal electric fields emerge, strongly related with many physical properties such as the electronic structure, local charge carrier distributions, and related electromagnetic features.[1]

This charge transfer promotes atomic rearrangements leading to the observed atomic couples oppositely charged in 2D projected images of the crystal structure along certain directions, known as dumbbells. In binary compounds, that is, *AB*, depending on the dumbbell orientation along a certain direction (usually referred to the growth direction) the material is said to have A- (cationic) or B- (anionic) polarity, influencing their growth and physical properties (see Figure 1, showing the dumbbell orientation in III−V and II−V semiconductor binary NWs along their growth direction).

Most known and employed semiconductor materials crystallize either in the cubic zinc-blende (ZB) structure or in the hexagonal wurtzite (WZ)[2] with $F\bar{4}3m$ and $P6_3mc$ space groups, respectively. An equivalence can be established when comparing the growth along the {111} and {0001} directions in the ZB and WZ structures, as then, both structures are only distinguishable by the bilayer stacking sequence, being ...*aAbBcCaAbBcC*... and ...*aAbBaAbBaAbB*... for ZB and WZ, respectively; as displayed in Figure 2 (more details on these crystalline structures are given in the Supporting Information) and in refs 3−5.

One should note that it is the lack of mirror symmetry in binary compounds which turns them into polar materials. Interestingly, the {111} planes in ZB and {0001} in WZ, both

Received: January 31, 2019
Revised: April 23, 2019
Published: April 30, 2019

Downloaded via ECOLE POLYTECHNIC FED LAUSANNE on May 19, 2019 at 12:17:36 (UTC).
See https://pubs.acs.org/sharingguidelines for options on how to legitimately share published articles.

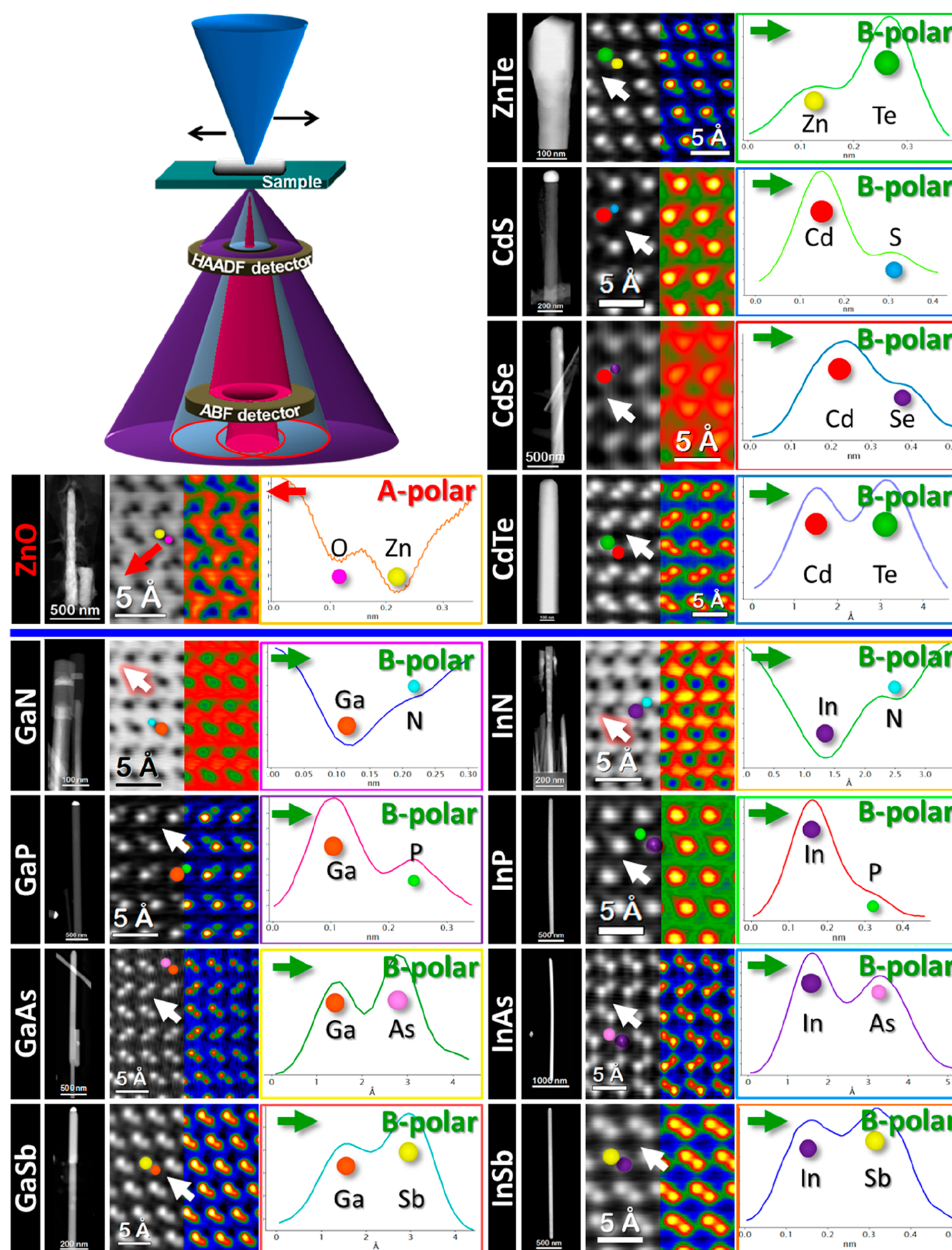

Figure 1. Main polarities observed on different semiconductor NW compounds. II−VIs (ZnO, ZnTe, CdS, CdSe, CdTe) and III−Vs (i.e., GaX and InX (X = N, P, As, Sb)) materials analyzed by aberration-corrected scanning transmission electron microscopy (STEM) techniques, as shown in the sketch. Low-magnification and atomic resolution HAADF(/ABF for the nitrides and ZnO) images of the analyzed NWs are displayed, along with intensity profiles along the dumbbells, following the arrow direction shown in the images. In the cases shown above, only ZnO grows along the A-polar direction while the rest do it along B-polar. All the images are vertically oriented along the NWs growth directions.

polar planes, are the typical growth fronts in semiconductor nanostructures. Within this context, two opposite polar orientations of the same crystal plane experience different growth rates,[6,7] determining for instance, the symmetry of core−multishell NWs,[8] which can be exploited for the formation of novel self-assembled quantum structures with advanced functional properties.[9−11] Additionally, opposite polar growth directions not only may alter the internal crystal structure features but also the overall nanostructure of the system. A- versus B-polar directed growths show distinctive defect concentrations[6,12,13] and impurity/doping incorporation rates, leading to nonuniform composition in ternary or quaternary systems, such as InGaAs or AlGaInAs NWs,[14,15] or changing the doping nature from n- to p-type when polarity is reversed.[16] The formation of transverse twins (perpendicular to the growth axis)[17] are common in B-polar NWs,[3] while A-polar NWs (e.g.. InP and GaAs) are free of transverse twins, although they might present a low density of lateral twins in B-polar directions (not perpendicular to the growth axis).[13,18] Twins indeed preferentially occur along B-polar directions for InP and GaAs, although they are preferred along A-polar directions in Sn-seeded GaSb nanowires.[19] It is important to point out that in nonpolar systems such as group IV semiconductors (e.g., Si, Ge) a combination of twins can coexist in the same structure, transverse and lateral,[17] due to the lack of polarity. The presence of twin boundaries is closely related to the formation of crystal polytypes, thus a high twin density increases the probability of obtaining the WZ structure.[3,20] The presence of ZB or WZ

DOI: 10.1021/acs.nanolett.9b00459
Nano Lett. XXXX, XXX, XXX−XXX

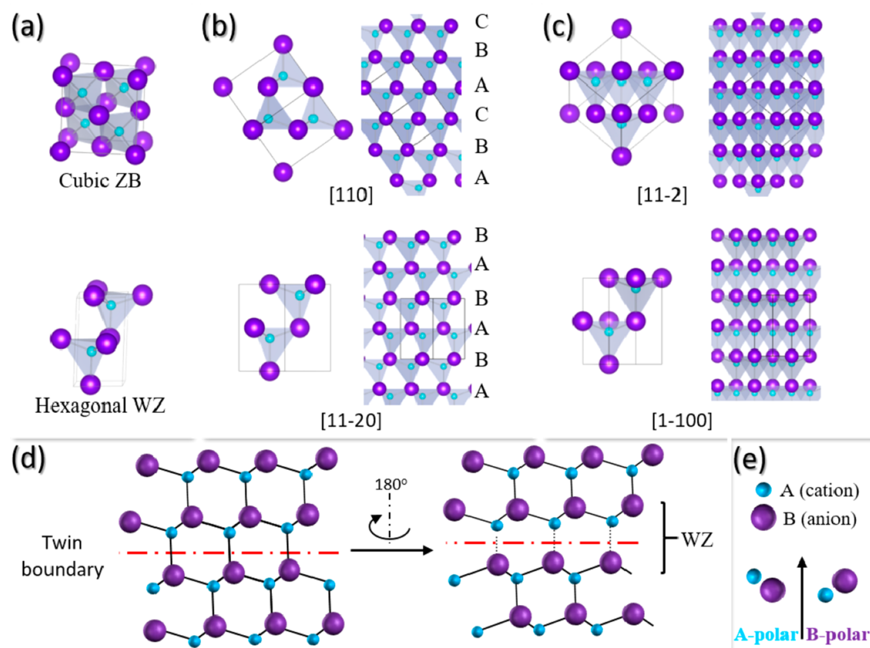

Figure 2. Schematics of the ZB and WZ structures. (a) Unit cells for the cubic ZB (top) and hexagonal WZ (bottom) phases. (b) The 2D projections of the ZB (top) and WZ (bottom) along the [110] and $[11\bar{2}0]$ zone axes for the ZB and WZ, respectively. (c) The 2D crystal projections along the $[11\bar{2}]$ and $[1\bar{1}00]$ for ZB (top) and WZ (bottom). (d) Pristine ZB structure (left-hand) and twinned ZB (right-hand), where the twin boundary is equivalent to a half monolayer of WZ. (e) A-polar and B-polar dumbbells, referring to the polarity along the arrow direction drawn between both dumbbells. In III–V and II-VIs compounds, A (cyan) is the III or II element, while B (purple) is the V or VI.

crystal phases in a nanostructure is strongly influenced by polarity.[13,18,19] In terms of the growing system geometry, the formation of different free-standing nanostructures such as NWs, tripods, tetrapods, nanomembranes, and so on,[21−25] as well as their orientation,[26] can be explained attending to polarity arguments. It is important to note that the term free-standing may refer to different situations, however, when used along the present work we refer to systems involving nanostructures growing vertically outward from a substrate in a nonplanar configuration with only a small portion of the nanostructure contacting the substrate.

Differences in the chemical and physical behavior of polar-oriented systems are remarkably relevant in the final applications. It is known that the same surface planes with opposite polarities exhibit different chemical behaviors and optoelectronic properties.[27,28] For instance, it has been shown that in InGaN/GaN quantum wells (QWs), the carrier localization and transport are dependent on the polarity.[29]

A further related issue regards the polarity preservation or inversion within a nanostructure. Although polarity inversions are thermodynamically unlikely in unidirectionally grown binary compounds, more complex morphologies or heterostructured systems may allow polarity inversions with dramatic implications on the transport and optical properties.[30,31]

The above-mentioned scenario shows that polarity imposes a further degree of freedom to functionalize binary semiconductor nanostructures, highlighting the importance to control the polarity along certain directions. Most binary compounds grow easily along the B-polar direction and A-polar growth is hardly achieved.[26] Still, there are a few controversial materials,[32−34] namely, InP, GaN, and ZnO, reported to follow either A- or B-polar directions. So far, systematic comparison between the different systems is challenging due to the many factors affecting the growth. This is partially due to the variety of growth techniques available to produce NWs, including chemical and physical methods, each of them requiring the proper environmental conditions for the growth to succeed. Thus, different substrates, temperatures, fluxes, precursors, doping, catalyst seeds, and so forth are involved, and relating their influence to the material polarity is not straightforward. Although polarity has been studied in several semiconductor binary systems, the reasons determining the final polarity of free-standing architectures are not yet well understood.

In order to find the underlying mechanism ruling the polar growth, we have analyzed the most commonly III–V and II–VI binary compounds synthesized as NWs. We have chosen aberration-corrected STEM to determine the polarity, which provides a reliable tool for this purpose.[16,30,35,36] Combining high-angle annular dark-field (HAADF) and annular bright-field (ABF) STEM techniques, we have been able to easily differentiate and identify the dumbbell constituents, even when dealing with compounds containing light elements, such in oxides (O) and nitrides (N),[30] to address the polarity of the growth plane (see Supporting Information for more details). The obtained results are compared to previously published data on the topic, opening the discussion on how different intrinsic material properties and extrinsic growth parameters may (or may not) induce a preferential polarity, paying special attention to those compounds following both opposite polar directions. Subsequently, we exemplify the relevance of the polarity-driven growth mechanisms that allow for the development of a wide variety of morphologies, such as free-standing branched/polypod architectures or 2D-like nanostructures. Finally, we devote the final section of the present work to illustrate possible polarity inversions in nanostructured semiconductor materials, discussing a few examples of inversion boundaries, which eventually allow a smart manifold functionalization of the

DOI: 10.1021/acs.nanolett.9b00459
Nano Lett. XXXX, XXX, XXX−XXX

Table 1. Reported Polar Directions for InP, GaN, InN, and ZnO Materials, Indicating the Type of the Growth Mechanism (Spontaneous, Selective Area, or Particle-Assisted Growths Are Distinguished)

material	polarity	references
InP	A (In)	Ikejiri et al.,[48] Poole et al.,[49] Gao et al.[50] → SAG
	B (P)	Algra et al.,[51] Dalacu et al.,[52] Calahorra et al.[53] → particle-assisted
GaN	A (Ga)	Schuster et al.,[33] Bengoechea-Encabo et al.[54] → SAG
	B (N)	Fernández-Garrido et al.,[55] Bertness et al.,[56] Schuster et al.[57] → particle-assisted Mußener et al.[58] → spontaneous growth
InN	A (In)	Wang et al.[59] → spontaneous growth
	B (N)	Stoica et al.,[60] Chang et al.,[61] Wang et al.[59] → spontaneous growth
ZnO	A (Zn)	Baxter et al.,[62] Sallet et al.,[63] Utama et al.,[64] Guillemin et al.,[65] Sun et al.,[66] Nicholls et al.[67] → spontaneous growth Scrymgeour et al.,[68] Perillat-Merceroz et al.,[69] Consonni et al.[70] → SAG Jasinski et al.[71] → particle-assisted
	B (O)	Guillemin et al.[72] → spontaneous growth Consonni et al.[70] → SAG Sallet et al.[63] → particle-assisted

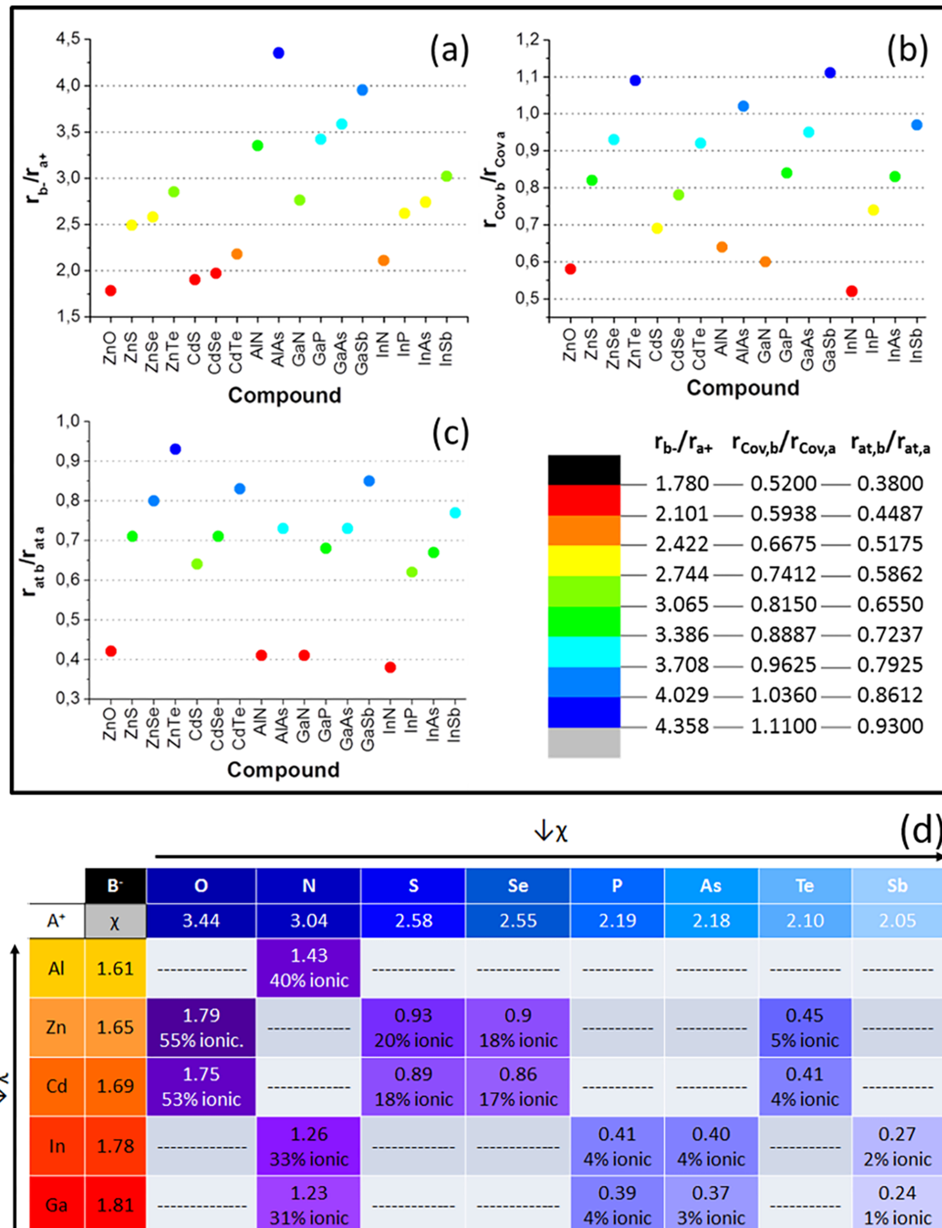

Figure 3. Intrinsic parameters of the binary compounds analyzed, such as the ratio between the constituent sizes (r_b/r_a), including the cases of ionic (a), covalent (b), and atomic radius, and the ionic character of the compound showing the electronegativity for each constituent, χ, along with the difference in electronegativity for every considered compound (d), calculated following Pauling's expression (more details provided in the Supporting Information).

optoelectronic properties of the nanostructures (polarity nanoengineering).

Polarity-Driven Growth of Vertical Nanowires. While semiconductor NWs have extensively been studied systems over

DOI: 10.1021/acs.nanolett.9b00459
Nano Lett. XXXX, XXX, XXX−XXX

the last years, the available research works usually focus on only one material system or a family of them (e.g., nitrides, arsenides, and so forth). Therefore, although there is a huge amount of literature on the growth of NWs and the polar growth, there are not well-established connections rendering a universal picture. In the following, we present our results in III−V and II−VI NWs and explore the possible effect of intrinsic crystal properties on the polar growth. Then, we discuss the role of the growth mechanism on the polar growth through few examples of systems reported to grow along two opposite polar directions.

Atomic Polarity Measurements. III−V Compounds. Among all possible III−V combinations, we have characterized GaX and InX NWs, where X = N, P, As, or Sb. Low-magnification STEM images for the different NWs, atomic resolution HAADF/ABF STEM images of their structure, and intensity profiles along dumbbells in each binary combination are included in Figure 1. Further details on the characterization methodology can be found in the Supporting Information. All the III−V NWs analyzed (bottom panel in Figure 1) grow along a B-polar direction, regardless of their crystalline phase.

Hence, all the NWs here studied belonging to any III−V combination grow along either $[000\bar{1}]$ in hexagonal WZ systems or any ⟨111⟩ B if the material has cubic ZB structure, in good agreement with most reported cases. In fact, there is a general belief supporting the preferential growth of III−V NWs following anionic polar directions.[37] This is, for instance, the most common trend observed in GaAs, which grows easily on B-polar substrates following B-polar directions. In contrast, it is usually observed that the use of A-polar substrates prevents the formation of vertical NWs for the growth conditions employed, whereas other substrate orientations lead to the formation of tilted NWs along the available ⟨111⟩B directions.[26] By growing the NWs on top of nonpolar substrates, such as Si, GaAs free-standing nanostructures have been found to easily form along B-polar directions. In some cases, complex growth paths involving the well-established 3D multiple-order twinning mechanism allow the NW to reach B-polar growth directions after *n* twinning events.[38] However, for very specific growth regimes the formation of III−V A-polar NWs can be successfully achieved.[6,13,18,19] Indeed, few III−V combinations, such as InP and GaN, may grow along A-polar directions in addition to B-polar ones. GaN is among the most controversial material in this sense and, actually, there are researchers supporting A-polar directed growth of GaN elongated nanostructures,[39−41] whereas some works claim the irrevocably B-polar nature of spontaneously formed NWs[42] (see Table 1). Even mixed polarities have been reported within the same batch of grown GaN NWs,[16] although with the majority (90%) of the NWs growing along the $[000\bar{1}]$ B-polar direction. Interestingly, B-polar growth remains a preference on Si(111) for most planar films of InAs, GaAs, and GaSb as well. Although in some cases, the authors claimed a control over polarity with interface engineering.[43,44]

II−VI Compounds. Turning now to II−VI combinations, we have determined the polarity in several Zn- and Cd-based chalcogenides presenting ZB-WZ polytypism. Compounds with other nonpolar phases are excluded from the study (as it is the case of CdO which usually shows rock-salt structure). The analyzed II−VI NWs comprise ZnO, ZnTe, CdS, CdSe, and CdTe. ZnO, CdS, and CdSe crystallize as pure WZ; CdTe NWs show polytypism from the base to the tip with short WZ and ZB axial segments of variable thicknesses, whereas ZnTe NWs have a twinned ZB structure (ZB with highly spaced twin boundaries).

Interestingly, among the chalcogenides, we find out that ZnO growth is directed by the cationic [0001] A-polar direction, whereas the other analyzed II−VI compounds follow the most commonly observed anionic growth, B-polar (top panel in Figure 1). Indeed, ZnO with both A- and B-polarities has been reported, analogous to the case of GaN in the III−V family (see Table 1).

Some intrinsic parameters of the constituent atoms of the material are known to affect its crystallinity. For instance, the ionicity is critical in the resulting atomic package, which is a property of the compounds related to the relative electronegativity between the constituents. Also, the atomic sizes of the elements conforming to the material have an important role on the resulting phase.

Polarity in binary compounds is an extra variable on its crystallinity. We have tried to correlate some atomic parameters of the constituents and geometrical factors of the phases with the experimental observed polarity.

Intrinsic Parameters That May Influence the Polar Growth. In order to understand the polarity-driven growth mechanism, we have first evaluated a variety of intrinsic properties of the compound constituents, such as the relative radii or the compound ionicity. Starting by the relative atomic size, no trend is observed explaining the experimental observations. As some compounds are more covalent while others have a stronger ionic character, ionic and covalent radii are also explored (see Figure 3a−c and tables provided in the Supporting Information). Interestingly, the ratios calculated for ZnO lie always within the lower values range, but the overall trends vary depending on the radii considered. Regrettably, we could not find a direct connection between the radii relationships and the most common polarities observed for those compounds in nonplanar semiconductor nanostructures.

Another relevant parameter to consider regards the dangling bonds of the material constituents considered by some authors.[45] Imposed by the tetrahedral coordination of the constituents within the WZ and ZB crystallographic phases, *A* and *B* species at the polar {111} growing planes will have one dangling bond each. In the case of III−V compounds, III-group species (*A*) have such dangling bonds empty and V-group elements (*B*) have them occupied by unshared electrons. On one hand, the presence of unshared electrons preserves the tetrahedral environment (tetrahedral bond geometry) around the *B* species. On the other hand, the existence of empty dangling bonds around *A* constituents results in a coordination configuration in between planar and tetrahedral. On the basis of these arguments, A-polar surfaces should be less favored due to the surface distortion involved and, thus, B-polar directions would be preferred. In the case of II−VI materials, these arguments would be invalidated due to their stronger ionic character, as explained elsewhere.[46] Although useful for the authors to correlate the etching behavior of oppositely polarized surfaces, the prevalence of the ionic character over the atomic configuration imposed by the dangling bonds does not rule the unidirectional polar growth of II−VI compounds, accordingly to our observations.

Related to the previous point analyzed, we try to extract some meaningful information by focusing on the ionic character of the considered compounds, which might affect the polarity. We use the differences in electronegativities between atomic constituents, $\Delta\delta$, as well as Pauling's ionicities (expressed in percent) for the binary compounds studied (see Figure 3d and Supporting Information for further details). Unfortunately, the $\Delta\delta$ or related

DOI: 10.1021/acs.nanolett.9b00459
Nano Lett. XXXX, XXX, XXX−XXX

ionicity does not explain the observed polarity on the NWs. Some of the cases reported to grow under A-polarity belong to the combinations with the highest ionicities, as ZnO or GaN, with 55 and 31% of ionic character on their bonding according to the calculations. However, the InP case, also reported to easily follow cationic directions while growing,[47] cannot be explained under this consideration, because its covalent bonds hardly reach a 4% of ionicity, invalidating any correlation of a favored polarity dependent on the ionic character of the compound.

So far, we could not find any consistent parameter that would relate the type of polarity with a group of binary semiconductors. This points out to the hypothesis that polarity might be mostly determined by the synthesis method and growth parameters used (i.e., temperature, pressure, III/V ratio, phases present during growth, nature of the catalyst seed etc.). Then, based on our results and previously reported data, it appears reasonable thinking that the observed polarity in free-standing nanostructures is a consequence of the parameters (conditions) used during the growth. Unfortunately, a complete comprehension of the dynamics and kinetics has not been achieved yet. Nevertheless, the growth parameters can be divided in two separated groups, depending on whether the growth is particle-assisted or not. This is further elaborated in the following.

Growth along A- and B-Polar Directions and the Effect of the Growth Mechanism. As commented above, few systems have been already reported to grow along two opposite polar directions. The most popular cases are InP, GaN, InN, and ZnO (see Table 1), discussed in the following attending to the underlying growth mechanism, that is, vapor−liquid−solid (VLS) or vapor−solid (VS).[73]

VLS-Related Growths. The VLS mechanism is a metal catalyst-assisted growth method (see further details in the Supporting Information) commonly employed to obtain semiconductor NWs. To the best of our knowledge, there is not a universal atomistic model that explains all types of particle-assisted NW growth. The growth is usually seeded by Au droplets or by group-III elements (self-catalyzed processes).

Apart from our observation of B-polar InP NWs, both, A- and B- polarities are reported in the literature (see Table 1). Interestingly, the reported B-polar InP NWs are grown by using metal seeds (particle-assisted growth).[74,75] Similarly, opposite polar directed growth of ZnO NWs has been reported depending on whether the growth is particle-assisted or not. Among other techniques, ZnO can be synthesized by metal−organic chemical vapor deposition (MOCVD) in both ways, particle-assisted and spontaneous growth modes, by tuning the growth parameters (mainly the O/Zn ratio). The resulting NWs show O-polarity whenever the synthesis is particle-assisted or VLS (see Table 1). Changing the synthesis from the chemical vapor transport to metal−organic vapor phase epitaxy (MOVPE), the growth of ZnO NWs on nonpolar and B-polar substrates has been achieved. Nevertheless, the spontaneously formed (catalyst free) NWs also follow the Zn-polar [0001] direction.[76] Another example of this preferential cationic polar growth occurs when the ZnO grows on top of GaN NWs, forming ZnO/GaN heterostructures. Even in this latter case, when growing the ZnO axially on top of the B(N)-polar GaN first grown stems, the ZnO shows A(Zn)-polarity.[77]

Hence, although it turns out that particle-assisted procedures tend to favor the B-polar directed growth, in agreement with our observations, the opposite A-polar direction is still possible under selected fine-tuned growth conditions.

VS-Related Growths. Whenever the use of a seed droplet is avoided, for example, by selective area growth (SAG), the preferred growth direction of InP is along an A-polar direction.[32,78] Note that the SAG procedure referred is governed by a VS mechanism (more details are provided in the Supporting Information), where the gas precursors directly impinge the solid substrate for the growth to proceed. In the case of ZnO NWs, they show Zn-polarity if they are spontaneously formed[79] (more details are provided in the Supporting Information).

In the case of GaN, using SAG conditions leads to the formation of A-polar GaN NWs,[33] as shown in Figure 4 (see also

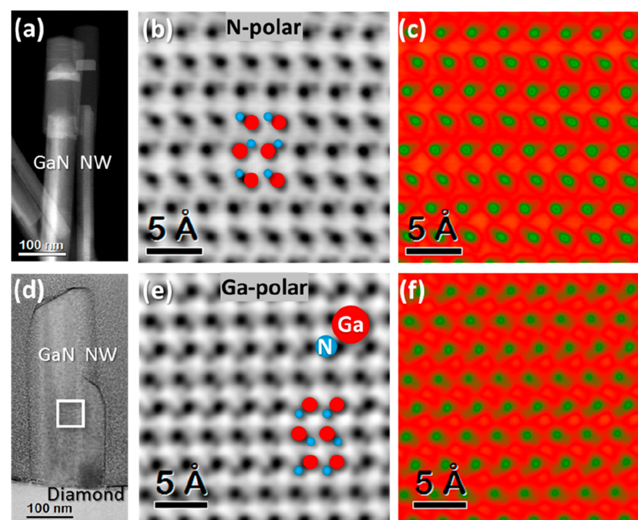

Figure 4. N- and Ga-polar GaN NWs. GaN NWs grown on Si substrate by PAMBE (a−c) and grown by SAG-PAMBE on diamond/Ti-substrate/mask (d−f). (a,d) Low-magnification HAADF image of the analyzed GaN NWs. (b,e) Atomic-resolution ABF image of the GaN phase shown by the NW included in (a,d), evidencing the N-/Ga-polar directed growth. False-colored images are displayed in (c,f).

Tables 1 and 2). By coating the diamond substrate with a patterned Ti mask the selective growth results in A-polar NWs,[33] contrary to their spontaneous formation on bare diamond substrates.[57] Morphological differences in NWs with opposite polar directions exist. A-polar NWs exhibit a much lower aspect ratio than B-polar NWs (see Figure 4). Such morphological differences may be indicative of the different dynamics/kinetics underlying the self-assembly and SAG procedures (more details in the Supporting Information). In some cases, we find in the literature other examples of SAG NWs with A-polarity, where the formation of A-polar nanowires is most probably not related to the SAG process but to the A-polarity of the substrate.[80]

The GaN NWs studied here are self-assembled on Si substrates, following a catalyst-free synthesis, following the vapor−solid (VS) mechanism instead of the VLS one, because there is not liquid droplet mediating the growth. Investigations on the growth of self-assembled GaN NWs within this regime claim the irrevocably B-polar nature of the NWs, irrespectively of the substrate polarity,[42] whereas B-polar substrates mostly lead to the formation of dense B-polar NW arrays; using A-polar substrates, sparse B-polar NWs are created on top of A-polar pedestals. A similar kind of growth is observed on nonpolar substrates, such as diamond.[81] The substrate orientation will define the growth angle (inclination) of the NWs. However, as long as the mismatch between the substrate and the NW

DOI: 10.1021/acs.nanolett.9b00459
Nano Lett. XXXX, XXX, XXX−XXX

Table 2. GaN Reported Growth Conditions and Polarity Found

reference	polarity	growth method	substrate	substrate coverage buffer/mask	temperature (°C)	V/III ratio	BEP_{Ga}(mbar)
Furtmayr et al.[83]	N	PAMBE	Si	Si_xN_y	775		3.9×10^{-7}
Schuster et al.[57]	N	PAMBE	C-diamond		930		
Schuster et al.[57]	Ga	SAG-PAMBE	C-diamond	Ti mask	890	71−500	4×10^{-7}
Cherns et al.[84]	Ga	PAMBE	sapphire	AlN buffer	700−800		
Alloing et al.[85]	N (∼73%)	MOVPE	sapphire		1100	20−200	
	N (mainly)	ammonia-MBE	sapphire		840		
	Ga (90%)	ammonia-MBE	Si	AlN	700		
Brubaker et al.[86]	Ga[a]	PAMBE	Si	AlN buffer	820 and 800[b]	1.0−1.03	
Lin et al.[87]	Ga	SAG-MOCVD	Si		1050−1175	12.6−2.1	
Carnevale et al.[88]	N (90%)	PAMBE	GaN(0001)	not mentioned	720 and 780[c]		
Carnevale et al.[89]	Ga	PAMBE	Si	not mentioned	720 and 780[c]		
Kong et al.[90]	N	PAMBE	Si	Si	700−800		
	Ga[d]	PAMBE	Si	AlN buffer	700−800		
Hestroffer et al.[91]	N	PAMBE	Si	Si_xN_y and AlN buffer	800	2.5	
den Hertog et al.[92]	N	PAMBE	Si		790		
Urban et al.[93]	Ga	SAG-PAMBE	GaN(0001)	Mo mask	780	9	
Fernández-Garrido et al.[55]	N	PAMBE	SiC(0001)	AlN buffer	815−825		
	N	PAMBE	SiC(0001)	AlN buffer	815−825		

[a]Mg-doped GaN NWs. [b]Two hours at 820 °C followed by 12 h at 800 °C. [c]Temperature of 720 °C for the nucleation and 780 °C for the growth. [d]Al_xGa_{1-x}XN NWs

material ensures a Volmer−Weber nucleation, the B-polarity will be kept.[82]

A summary table gathering different growth procedures for GaN NWs and the resulting polarity is provided (see Table 2). A more extensive review on GaN and ZnO polarity can be found in ref 94.

The case of InN is fairly similar to GaN, although reports on the actual unidirectional polar growth of InN are scarce for the InN case. InN NWs are also mainly synthesized catalyst-free by PAMBE under N-rich conditions, as GaN NWs, but at lower temperatures to prevent InN decomposition. MOVPE growth through self-catalyzed procedure has been recently reported to lead to N-polar InN NWs, too.[95] The parallelism between these III-nitrides is obvious, suggesting that they share the growth mechanism as expected from the similar growth procedures employed and thus the same polar behavior.

In the case of ZnO, the growth NWs is highly favored on A-polar substrates, as can be inferred from reported studies using periodically polarity-inverted substrates,[96−98] where the ZnO NW growth only succeeds on cationic-polar substrate regions. Such studies, included in refs 96−98, report Zn-polar NWs grown by chemical vapor transport and condensation from ZnO powder using Au particles as nucleation seeds[96] or by a catalyst-free procedure (more details in the Supporting Information).[97,98]

In contrast to what is reported elsewhere,[76] Consonni et al.[99] have shown that ZnO NWs follow the substrate polarity if they are selectively grown by chemical bath deposition (CBD), meaning that the Zn- or O- substrate polarity is transferred to the NWs. As the growth proceeds in solution phase, the main interactions to be considered during the growth are quite different from those on vapor phase. More details on the solution growth of ZnO NWs are provided in the Supporting Information.

Taking into account our experimental observations and previous studies, it is likely that the unidirectional polarity-driven growth at the nanoscale is a consequence of the underlying mechanism promoting the growth, which is dependent on the synthesis procedure and experimental conditions. It should be therefore possible to find the proper synthesis conditions favoring growth along cationic polar directions for any compound (A-polar), in addition to the most commonly observed anionic-polar growth, as it has been already observed for few systems, as InP, GaN (and InN), ZnO, or GaAs.

Polarity-Driven Morphological Transitions. From the previous observation of NWs growing with a preferred polarity, which is conserved along the whole length, one can state that nucleation at the substrate with a favored polarity may regulate the yield of NWs. However, the synthesis of more complex morphologies is also possible and their formation can be understood also attending to polarity arguments, along with polytypism and twinning phenomena.

Branched Nanostructures. Among the different morphologies attainable, branched nanostructures with different number of legs are commonly reported in binary (AB) semiconductor materials, as for instance tripods and tetrapods. When obtained epitaxially on top of a substrate, these nanostructures are perfectly aligned with each other[22,33] even in the case of van der Waals incommensurate epitaxy (see Supporting Information).[100] Insights on their crystalline structure and polarity provide key information on the growth mechanisms.

The proposed growth mechanism for tripods is similar for the different binary compounds.[21,32,101] The central part of the tripods (namely the core), where the legs or ramifications merge together, crystallizes under pristine ZB structure, while the legs usually show a polytypic mixture with predominating existence of WZ (Figure 5a). This mechanism is known as polytypic branching.[102,103] Despite the changes on the crystal phase between the different parts (core and legs), they are coherently attached, as it can be seen when properly orienting the tripods along the $[\bar{1}0\bar{1}]$core∥ [110]legs or $[11\bar{2}0]$legs (depending on the considered phase for the legs, ZB or WZ). Therefore, the system evolves by the creation of different legs growing along the ⟨0001⟩ direction of the WZ phase, initiated at {111} planes of the ZB core following the most favored polar-direction for the employed growth conditions. This means that, for instance, in the case of ZnTe or GaN tripods growing at similar conditions

DOI: 10.1021/acs.nanolett.9b00459
Nano Lett. XXXX, XXX, XXX−XXX

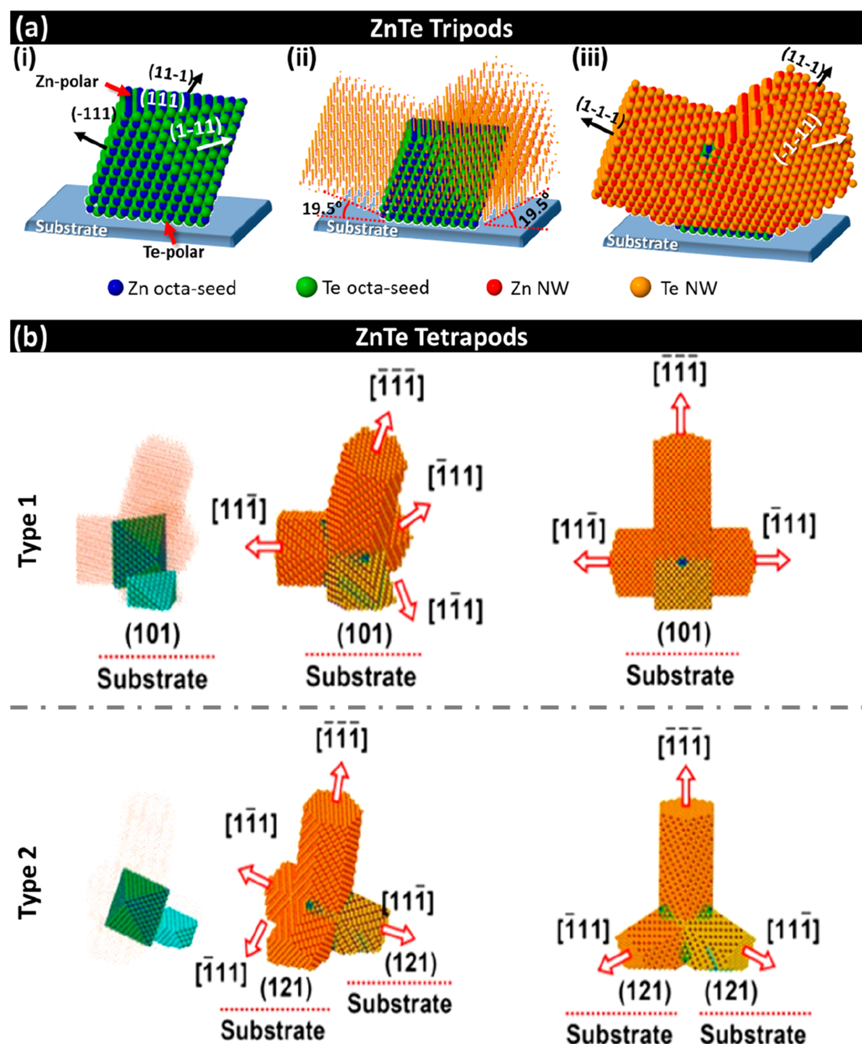

Figure 5. Atomic 3D models for the growth of tripods and tetrapods. (a) ZnTe tripods and (b) tetrapods. In both cases, the growth starts by the nucleation of octahedral seeds, either Zn-polar (a) or truncated by nonpolar planes (b), allowing the elongation of the legs along the available B-polar directions (favored polarity for the used growth conditions). Adapted from ref 22. Copyright (2013) WILEY-VCH.

than Te/Ga-polar NWs, they lengthen also along Te/Ga-polar directions, determined by the nucleation seeds. It is important to note that as there is a preferred polar elongation direction, NWs and tripods necessarily grow from oppositely polarized nucleation seeds, keeping the polarity at the core/leg interface[22,33] for the growth to succeed (further details on the growth mechanism are available in the Supporting Information). Slightly different considerations may be taken into account to explain the formation of tetrapods (Figure 5b), whose legs also grow following the favored polarity (growth mechanism described at the Supporting Information.

Driven by the most stable polarity under the growth conditions employed, the formation of NWs and tripods of different materials can be explained based on similar models than the one proposed.[21,32,101,104] Another example illustrating such fact can be found in GaN nanostructures. Growth conditions propitious to A-polar growth, lead to A-polar NWs, tripods, and nanotubes.[33] This is the case of growth on diamond by SAG. Similarly, InP tripods grown following selective-area metalorganic vapor-phase epitaxy (SA-MOVPE) procedures where the growth along A-polar directions is favored versus B-polar ones.[32]

Additionally, branched structures with multiple legs can be obtained in liquid solution by following similar polarity rules as polytypic branching occurs[105] (more details and a further discussion can be found in the Supporting Information).

Free-Standing 2D Nanostructures. Further related cases of polarity driven-growth mechanisms can be found in vertical 2D belts, flakes, or nanomembranes. The anisotropic growth behavior along opposite (0001) polar directions has been noticed when growing ZnO,[106] ZnS,[107] CdS,[108] or CdSe[109] nanobelts or nanoribbons by thermal evaporation. In all those studies, the nanobelts grow laterally constricted by $\{000\pm1\}$ planes, which show comblike or sawtooth morphologies asymmetrically developed. The (0001) (A-polar) side tends to show saw/comb-teeth shape while the $(000\bar{1})$ (B-polar) side of the belts is more prone to remain flat. This fact is mainly attributed to the higher reactivity known for the A-polar surfaces compared to the B-polar ones. In contrast, under different growth conditions Te-terminated (B-polar) surfaces experience higher growth rates explaining the asymmetric development of some other ZnTe nanobelts.[110] On the basis of the observation of Zn enrichment on the growth front, the teeth formation on A-polar (0001) surfaces is believed to follow a self-catalytic process. For the ZnO and CdS cases, formation of nanofingers

DOI: 10.1021/acs.nanolett.9b00459
Nano Lett. XXXX, XXX, XXX−XXX

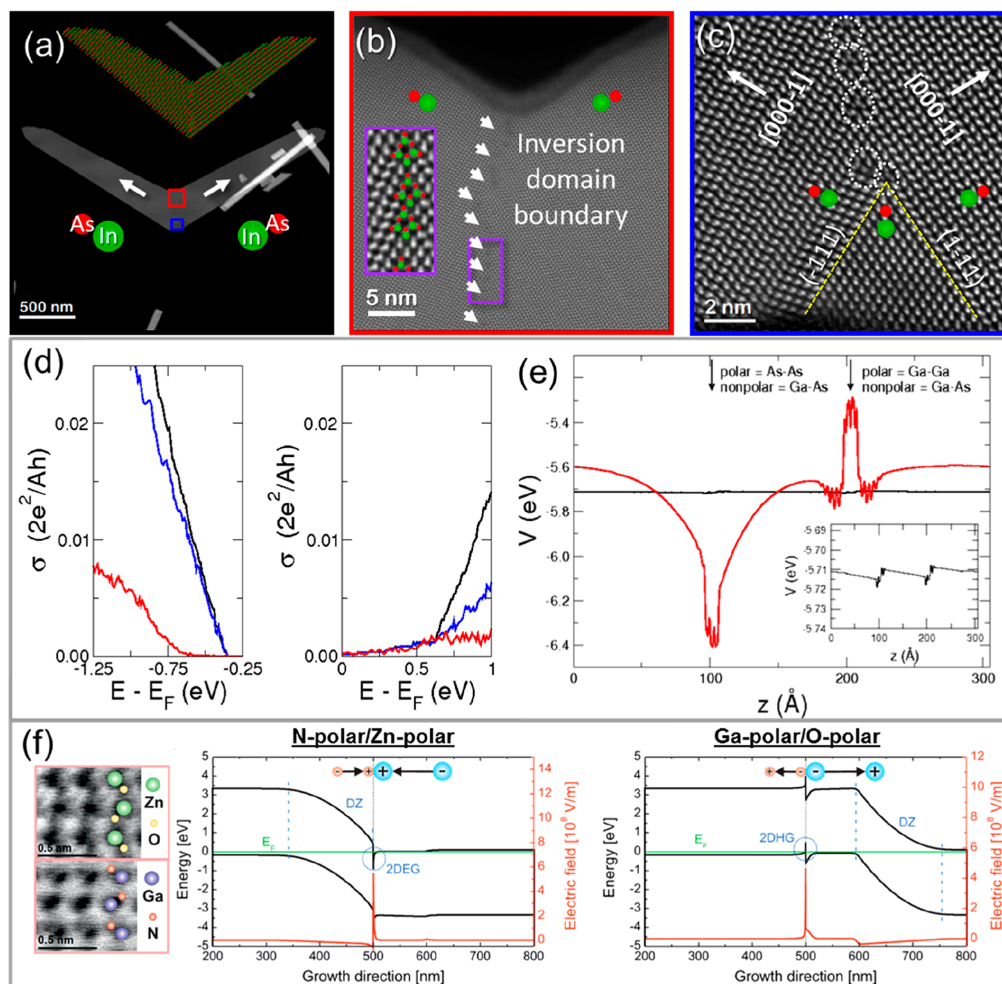

Figure 6. Polarity inversion. (a−c) Top panel: InAs V-shaped membrane growing from the center outward, developing the shape shown in (a). Atomic-resolution HAADF measurements evidence the dumbbell orientation in the central part of the architecture both at the top region where both branches merge together, leading to the inversion domain boundary (b) and at the base (c). (d,e) Middle panel: DFT calculations on the conductivity and electrostatic potential for GaAs. (d) Conductivity at the band edges for pristine GaAs (black), GaAs with two orthotwins (blue), and on GaAs with the presence of both paratwin configurations (red). (e) Electrostatic potential as perpendicular to the twin plane for presence of orthotwins (black) and paratwins (red). The arrows point at the twin location. Inset: magnification of the electrostatic potential in the presence of orthotwins. Figure adapted from ref 30. (f) Bottom panel: Polarity inversion experimentally observed at a GaN/ZnO heterostructured NW. The corresponding calculated 1D band structure (left axis) and electric field (right axis) for two different polar heterointerfaces (N-polar/Zn-polar and Ga-polar/O-polar) are also included, adapted with permission from ref 31. Copyright (2014) American Chemical Society.

on the anionic polar side can take place depending on the growth temperature.[106] The nanofingers are shorter and thinner than the sawteeth and are only formed at the lower-temperature regime. Although some of the nanobelts were synthesized by the particle-assisted procedure, the teeth formation occurs apart from the droplet, thus, through the vapor−solid mechanism. Another example of the asymmetric development of nanobelts is found in ZnTe extended sheets synthesized by vapor transport, which experience different growth rates at their lateral facets related to oppositely polar orientations.[110] Polarity arguments along with the observation of systematic particular defects have been used to explain the shape transition observed in InAs/InSb system.[24] While most of the developed architectures are axial heterostructured NWs, following B-polar directions in both phases, a non-negligible part of the nanostructures evolve toward vertical membrane-like shapes, also named nanosails. InSb ZB NWs usually grow on top the InAs WZ stems. The InSb NW section is limited by lateral {110} nonpolar facets, preventing the lateral expansion or overgrowth of the NW. However, after switching from InAs to InSb, the catalyst droplet may eventually wet a NW sidewall, allowing the nucleation of a lateral twin boundary at the transition interface. This twin boundary breaks the symmetry of the structure, creating a new {111}B lateral facet that will allow the lateral expansion of the nanostructure while keep on growing axially.

Therefore, under certain growth conditions a specific polarity drives the growth direction and, consequently, different morphologies can be obtained. As the fine-tuning of the growth conditions may switch the preferential polar direction, inducing such polarity at will in the growing material offers a powerful nanoengineering tool for the design of multiple morphologies.

So far, all the examples here reviewed deal with architectures where the polarity is never reversed. However, polarity inversions may be possible in certain systems, as we address in the following, with strong implications on the physical properties.

Polarity Inversions. WZ and ZB structures are prone to the presence of twin boundaries (see Supporting Information for

DOI: 10.1021/acs.nanolett.9b00459
Nano Lett. XXXX, XXX, XXX−XXX

more details), which are planar defects involving a lattice rotation of 180°, either perpendicular or around its normal vector.[111] Such crystallographic defects may reverse the polarity in addition to alter the atomic stacking sequence giving rise to intermediate polytypes.[112] It should be mentioned that to the best of our knowledge, no polarity inversions within pure binary NWs induced by twin defects have been reported. However, the presence of polar defects has been observed in other scenarios, as a consequence of doping, branching, or material combinations, as described below.

InAs V-shaped nanomembranes, which grow vertically on the substrate, are a typical example of an inversion domain boundary (IDB).[23] The membranes show a pyramidal nucleus of pure ZB at the central part of the base and two extended wings, of polytypic InAs phase growing outward the nucleus. The InAs ZB triangular projection of the nucleus grows along the [001] direction following the underlying Si substrate orientation, while standing on its (001) basal plane in contact with the Si surface and being laterally faceted by As-polarized {111} planes (Figure 6c). Thus, the membrane expansion proceeds along the anionic polar $[000\bar{1}]$ directions lying on the two lateral {111}B facets of the prismatic nucleus, inducing the branching of the structures into two "wings", both with B-polarity pointing the tips. During their lateral growth, the membranes keep on growing vertically to the substrate, too. As a consequence, above the top vertex of the prismatic triangular nuclei, there is an interaction region where the two wings merge together (Figure 6b). The growth of the wings along B-polar directions results in the convergence of two A-polar domains facing each other, as shown in Figure 6b,c. Therefore, an antiphase boundary defect propagates perpendicularly to the substrate along the membranes, starting from the top vertex of the ZB triangular seed, and dividing the membranes into two polar domains. The configuration or atomic arrangement of the IDB is dependent on the polytypic stacking sequences of the regions merging at both sides of the defect. The presence of pure WZ segments at both sides of the boundary leads to the formation of straight defects, while twinning and polytypic mixtures results in local deviations of the IDB trajectory. There are three possible dumbbell orientations in the structures, derived from the branching and the polytypism phenomena. The boundary acts as a mirror defect with dumbbells oppositely oriented at both sides, and vertically aligned dumbbells are allowed in all the different regions, usually connecting both wings (Figure 6c). When the two matching regions are purely WZ, the atomic arrangements at the boundary locations consist of ring-like formations composed by six atoms, alternating As and In, conforming the IDB. Again, depending on the polytypic sequence, other atomic rearrangements are observed.

It is important to note that the IDB does not extend through the ZB nucleus at the base of the membranes. There, the polarity reversal is stepped, mediating the presence of the ZB, where all the dumbbells are vertically aligned. Such situation might induce different physical behavior on the different areas of the membranes, that is, the base containing the ZB nucleus or the upper merging area between the wings. Therefore, in addition to the polarity inversion among the wings of the membranes, one should account for the vertical asymmetry of the system.

Notice that, as a consequence of the preferential unidirectional polar growth, anionic in this case, the branched nanostructures develop an inversion domain boundary defect not observed in impurity free binary NWs. The effect of a polarity reversal on the electronic properties may be comparable to that reported for the inversion promoted by a paratwin within a GaAs NW.[30] Plain differences are predicted for the electron transport in the presence of nonpolar and polar twins. The theoretical calculations accounting for a paratwin (polar defect) and an orthotwin (nonpolar defect) by taking GaAs as the model system under three different considerations: occurrence of orthotwins and two possible paratwin configurations, that is, mirror twin creating a Ga−Ga bilayer and another for the As−As bilayer, as reported elsewhere.[30] The performed first-principles electron transport calculations in the ballistic regime by density functional theory (DFT) using the Siesta code[113] are summarized in the middle panel of Figure 6.

It is easily observed that the conductivity (Figure 6d) at the band edges is expected to dramatically drop if a polar paratwin (red curve) occurs compared with the pristine material (black curve), whereas the effect of the nonpolar orthotwin (blue curve) would almost not perturb the conductivity. Differences between polar and nonpolar twins are even more pronounced in the electrostatic potential (Figure 6e), which remains almost unchanged in the presence of orthotwins but is strongly modified if the twin inverts the polarity. Moreover, clear differences for the electron and hole conductivity can be seen as the As−As paratwin imposes a barrier for the holes, while the sharp barrier exhibited by the Ga−Ga paratwin scatters the electrons. This is true for defective homostructures, but even more for heterostructures where the different polarization leads to interface charges which strongly modify the band alignments depending on the polarity at both sides of the heterointerface.[31] The unavoidable discontinuity on the band structures when switching the material, that is, at the interface, can be exploited to create two-dimensional electron gases, two-dimensional hole gases (see Figure 5f), or tunnel diodes, for instance, by properly adjusting with the polarity at both sides of the interface. In the particular case of GaN/ZnO NWs, it has been experimentally found that A-polar ZnO may grow on top of B-polar GaN stems, resulting in an inversion domain heterojunction, where the N and O anions face each other.

In conclusion, we have found that NWs growing at the triple phase line, involving solid, liquid, and vapor phases (VLS growth), tend to follow mainly B-polar directions in both III−V and II−VI compounds. The liquid phase is usually intentionally present in the medium by using metallic catalyst particles which will act as nucleation seeds. In addition, the metallic species supplied during the growth, that is, III- and II-group species, can result on the formation of liquid droplets with the same effects on the overall procedure (self-catalytic mode). These metallic droplets collect the supplied vapor species which will arrive by diffusion on the substrate and NW sidewalls in the case of metals (III and II species) or by impinging the droplet and diffusing through the interface with the substrate (during the nucleation)/NW (alternatively nonmetallic species can be directly incorporated at the triple phase line, as in the case of oxygen), for the V and VI elements.

On the contrary, under certain growth conditions it is possible to force the A-polar growth by using A-polar substrates, and/or increasing the III/V ratios during the growth, even on unpolar substrates. In this way, a delicate control on the experimental conditions and on how they rule the growth is essential, since their modification can switch the growth regime resulting in a different mechanism, and thus, losing the control over the polarity. The known possibility for some materials to grow under both polarities is encouraging for the general case to be accessible to polarity engineering by finding the proper growth

DOI: 10.1021/acs.nanolett.9b00459
Nano Lett. XXXX, XXX, XXX−XXX

conditions. It is worth keeping in mind that the requirement to be fulfilled is enhancing one polar growth over the other, making the desirable polar direction being developed faster than the opposite and hence, driving the obtained morphology. More work should be done to reach the desirable understanding on the growth, because even for the widely employed VLS procedure a complete comprehension of the process has not been achieved yet.

Outlook. Aiming to shed light over the mechanisms determining the growth polarity at the nanoscale, we have extensively employed atomic resolution STEM-related methodologies in order to determine the polarity in the most commonly synthesized and used III-Vs and II-VIs nanostructures, creating a complete mapping of the resulting preferential polarities. Despite the finding that the vast majority of the nonplanar semiconductor nanostructures follow anionic or B-polar directions, few materials show the versatility in growing in both A- and B-polar directions (e.g., GaN, InP, ZnO) and hence open the discussion on the feasibility of predetermining the desirable polarity during growth for any compound material.

It is noteworthy that the growth procedures leading to opposed polar growths (A- and B-polar nanostructures) are governed by different thermodynamics and/or kinetics than those reported to exclusively lead to B-polar nanostructures. Thus, we provide an overview of the extrinsic parameters tunable during the growth and how they influence the polarity-driven growth at the nanoscale. The fine control over polarity in semiconductor materials broadens the possibilities on the design of novel morphologies and might allow the creation of newly developed quantum devices, based on the smart construction of polarity inversions at will, in both homo- and heterostructures.

■ ASSOCIATED CONTENT

Supporting Information

The Supporting Information is available free of charge on the ACS Publications website at DOI: 10.1021/acs.nanolett.9b00459.

Additional information including experimental details and methods, additional figures, and additional references (PDF)

■ AUTHOR INFORMATION

Corresponding Authors

*E-mail: maria.delamata@uca.es.

*E-mail: arbiol@icrea.cat.

ORCID

María de la Mata: 0000-0002-1581-4838

Reza R. Zamani: 0000-0001-6940-0000

Qihua Xiong: 0000-0002-2555-4363

Anna Fontcuberta i Morral: 0000-0002-5070-2196

Jordi Arbiol: 0000-0002-0695-1726

Present Address

◆(M.d.l.M) Departamento de Ciencia de los Materiales, Ing. Met. y Qca. Inorg., IMEYMAT, Universidad de Cádiz, 11510 Puerto Real, Spain.

Notes

The authors declare no competing financial interest.

■ ACKNOWLEDGMENTS

ICN2 acknowledges funding from Generalitat de Catalunya 2017 SGR 327 and the Spanish MINECO coordinated project ENE2017-85087-C3. ICN2 is supported by the Severo Ochoa program from Spanish MINECO (Grant SEV-2017-0706) and is funded by the CERCA Programme/Generalitat de Catalunya. Part of the present work has been performed in the framework of Universitat Autònoma de Barcelona Materials Science Ph.D. program. S.M.S. acknowledges funding from "Programa Internacional de Becas "la Caixa"-Severo Ochoa". The HAADF-STEM experiments were conducted in the Laboratorio de Microscopias Avanzadas at Instituto de Nanociencia de Aragon-Universidad de Zaragoza. A.F.i.M. thanks SNSF for funding through the NCCR QSIT. This work has received funding from the European Union's Horizon 2020 Research and Innovation Programme under grant agreement No. 654360 NFFA-Europe. This project has received funding from the European Union's Horizon 2020 research and innovation programme under grant agreement No. 823717 – ESTEEM3.

■ REFERENCES

(1) Nakamura, S. *MRS Bull.* **2009**, *34*, 101–107.

(2) Arbiol, J.; Fontcubertai Morral, A.; Estrade, S.; Peiro, F.; Kalache, B.; Rocai Cabarrocas, P.; Morante, J. R. *J. Appl. Phys.* **2008**, *104*, 064312.

(3) Spirkoska, D.; Arbiol, J.; Gustafsson, A.; Conesa-Boj, S.; Glas, F.; Zardo, I.; Heigoldt, M.; Gass, M. H.; Bleloch, A. L.; Estrade, S.; Kaniber, M.; Rossler, J.; Peiro, F.; Morante, J. R.; Abstreiter, G.; Samuelson, L.; Fontcuberta i Morral, A. *Phys. Rev. B: Condens. Matter Mater. Phys.* **2009**, *80*, 245325.

(4) Arbiol, J.; Estradé, S.; Prades, J. D.; Cirera, A.; Furtmayr, F.; Stark, C.; Laufer, A.; Stutzmann, M.; Eickhoff, M.; Gass, M. H.; Bleloch, A. L.; Peiró, F.; Morante, J. R. *Nanotechnology* **2009**, *20*, 145704.

(5) Caroff, P.; Bolinsson, J.; Johansson, J. *IEEE J. Sel. Top. Quantum Electron.* **2011**, *17*, 829–846.

(6) Wacaser, B. A.; Deppert, K.; Karlsson, L. S.; Samuelson, L.; Seifert, W. *J. Cryst. Growth* **2006**, *287*, 504–508.

(7) Burgess, T.; Breuer, S.; Caroff, P.; Wong-Leung, J.; Gao, Q.; Tan, H. H.; Jagadish, C. *ACS Nano* **2013**, *7*, 8105–8114.

(8) Zheng, C.; Wong-Leung, J.; Gao, Q.; Tan, H. H.; Jagadish, C.; Etheridge, J. *Nano Lett.* **2013**, *13*, 3742–3748.

(9) Heiss, M.; Fontana, Y.; Gustafsson, A.; Wüst, G.; Magen, C.; O'Regan, D. D.; Luo, J. W.; Ketterer, B.; Conesa-Boj, S.; Kuhlmann, A. V.; Houel, J.; Russo-Averchi, E.; Morante, J. R.; Cantoni, M.; Marzari, N.; Arbiol, J.; Zunger, A.; Warburton, R. J.; Fontcuberta i Morral, A. *Nat. Mater.* **2013**, *12*, 439–444.

(10) de la Mata, M.; Zhou, X.; Furtmayr, F.; Teubert, J.; Gradečak, S.; Eickhoff, M.; Fontcubertai Morral, A.; Arbiol, J. *J. Mater. Chem. C* **2013**, *1*, 4300–4312.

(11) Arbiol, J.; Dela Mata, M.; Eickhoff, M.; Fontcuberta i Morral, A. *Mater. Today* **2013**, *16*, 213–219.

(12) Hughes, S. M.; Alivisatos, A. P. *Nano Lett.* **2013**, *13*, 106–110.

(13) Yuan, X.; Caroff, P.; Wong-Leung, J.; Fu, L.; Tan, H. H.; Jagadish, C. *Adv. Mater.* **2015**, *27*, 6096–6103.

(14) Guo, Y.-N.; Burgess, T.; Gao, Q.; Tan, H. H.; Jagadish, C.; Zou, J. *Nano Lett.* **2013**, *13*, 5085–5089.

(15) Francaviglia, L.; Tütüncüoglu, G.; Martí-Sánchez, S.; Di Russo, E.; Escobar Steinvall, S.; Segura Ruiz, J.; Potts, H.; Friedl, M.; Rigutti, L.; Arbiol, J.; Fontcuberta i Morral, A. *Phys. Rev. Mater.* **2019**, *3*, 023001.

(16) Carnevale, S. D.; Kent, T. F.; Phillips, P. J.; Sarwar, A. T. M. G.; Selcu, C.; Klie, R. F.; Myers, R. C. *Nano Lett.* **2013**, *13*, 3029–3025.

(17) Conesa-Boj, S.; Zardo, I.; Estradé, S.; Wei, L.; Alet, P. J.; Roca i Cabarrocas, P.; Morante, J. R.; Peiró, F.; Fontcuberta i Morral, A.; Arbiol, J. *Cryst. Growth Des.* **2010**, *10*, 1534–1543.

(18) Zamani, M.; Tütüncüoglu, G.; Martí-Sánchez, S.; Francaviglia, L.; Markov, E.; Kim, W.; Güniat, L.; Ghisalberti, L.; Potts, H.; Friedl, M.; Leran, J.-B.; Dubrovskii, V. G.; Arbiol, J.; Fontcuberta i Morral, A. *Nanoscale* **2018**, *10*, 17080–17091.

(19) Zamani, R. R.; Ghalamestani, S. G.; Niu, J.; Skölda, N.; Dick, K. A. *Nanoscale* **2017**, *9*, 3159–3168.

DOI: 10.1021/acs.nanolett.9b00459
Nano Lett. XXXX, XXX, XXX–XXX

(20) Heiss, M.; Conesa-Boj, S.; Ren, J.; Tseng, H.-H.; Gali, A.; Rudolph, A.; Uccelli, E.; Peiró, F.; Morante, J. R.; Schuh, D.; Reiger, E.; Kaxiras, E.; Arbiol, J.; Fontcuberta i Morral, A. *Phys. Rev. B: Condens. Matter Mater. Phys.* **2011**, *83*, 045303.
(21) Utama, M. I. B.; Zhang, Q.; Jia, S.; Li, D.; Wang, J.; Xiong, Q. *ACS Nano* **2012**, *6*, 2281−2288.
(22) Utama, M. I. B.; Dela Mata, M.; Magen, C.; Arbiol, J.; Xiong, Q. *Adv. Funct. Mater.* **2013**, *23*, 1636−1646.
(23) Conesa-Boj, S.; Russo-Averchi, E.; Dalmau-Mallorqui, A.; Trevino, J.; Pecora, E. F.; Forestiere, C.; Handin, A.; Ek, M.; Zweifel, L.; Wallenberg, L. R.; Rüffer, D.; Heiss, M.; Troadec, D.; Dal Negro, L.; Caroff, P.; Fontcuberta i Morral, A. *ACS Nano* **2012**, *6*, 10982−10991.
(24) Dela Mata, M.; Leturcq, R.; Plissard, S. R.; Rolland, C.; Magén, C.; Arbiol, J.; Caroff, P. *Nano Lett.* **2016**, *16*, 825−833.
(25) Güniat, L.; Martí-Sánchez, S.; Garcia, O.; Boscardin, M.; Vindice, D.; et al. *ACS Nano* **2019**, DOI: 10.1021/acsnano.9b01546.
(26) Fontcubertai Morral, A.; Colombo, C.; Abstreiter, G.; Arbiol, J.; Morante, J. R. *Appl. Phys. Lett.* **2008**, *92*, 063112.
(27) Urban, A.; Malindretos, J.; Simon, P. *New J. Phys.* **2013**, *15*, 053045.
(28) Losurdo, M.; Giangregorio, M. M. *Appl. Phys. Lett.* **2005**, *86*, 091901.
(29) Lai, Y.-L.; Liu, C.-P.; Lin, Y.-H.; Lin, R.-M.; Lyu, D.-Y.; Peng, Z.-X.; Lin, T.-Y. *Appl. Phys. Lett.* **2006**, *89*, 151906.
(30) Dela Mata, M.; Magen, C.; Gazquez, J.; Utama, M. I. B.; Heiss, M.; Lopatin, S.; Furtmayr, F.; Fernández-Rojas, C. J.; Peng, B.; Morante, J. R.; Rurali, R.; Eickhoff, M.; Fontcubertai Morral, A.; Xiong, Q.; Arbiol, J. *Nano Lett.* **2012**, *12*, 2579−2586.
(31) Schuster, F.; Laumer, B.; Zamani, R.; Arbiol, J.; Stutzmann, M.; et al. *ACS Nano* **2014**, *8*, 4376−4384.
(32) Ikejiri, K.; Ishizaka, F.; Tomioka, K.; Fukui, T. *Nano Lett.* **2012**, *12*, 4770−4774.
(33) Schuster, F.; Hetzl, M.; Weiszer, S.; Garrido, J. A.; Dela Mata, M.; Magen, C.; Arbiol, J.; Stutzmann, M. *Nano Lett.* **2015**, *15*, 1773−1779.
(34) Consonni, V.; Sarigiannidou, E.; Appert, E.; Bocheux, A.; et al. *ACS Nano* **2014**, *8*, 4761−4770.
(35) Hertog, M. D.; Elouneg-Jamroz, M.; Bellet-Amalric, E.; Bounouar, S.; Bougerol, C.; André, R.; Genuist, Y.; Poizat, J. P.; Kheng, K.; Tatarenko, S. *J. Phys.: Conf. Series.* **2011**, *326*, 012044.
(36) Zamani, R.R.; Arbiol, J. *Nanotechnology* **2019**, *30*, 262001.
(37) Plissard, S.; Dick, K. A.; Larrieu, G.; Godey, S.; Addad, A.; Wallart, X.; Caroff, P. *Nanotechnology* **2010**, *21*, 385602.
(38) Uccelli, E.; Arbiol, J.; Magen, C.; Krogstrup, P.; Russo-Averchi, E.; Heiss, M.; Mugny, G.; Nyg, J.; Morante, J. R.; Fontcubertai Morral, A.; et al. *Nano Lett.* **2011**, *11*, 3827−3832.
(39) Cherns, D.; Meshi, L.; Griffiths, I.; Khongphetsak, S.; Novikov, S. V.; Farley, N.; Campion, R. P.; Foxon, C. T. *Appl. Phys. Lett.* **2008**, *92*, 121902.
(40) Alloing, B.; Vézian, S.; Tottereau, O.; Vennegues, P.; Beraudo, E.; Zuniga-Pérez, J. *Appl. Phys. Lett.* **2011**, *98*, 011914.
(41) Brubaker, M. D.; Levin, I.; Davydov, A. V.; Rourke, D. M.; Sanford, N. A.; Bright, V. M.; Bertness, K. A. *J. Appl. Phys.* **2011**, *110*, 053506.
(42) Fernández-Garrido, S.; Kong, X.; Gotschke, T.; Calarco, R.; Geelhaar, L.; Trampert, A.; Brandt, O. *Nano Lett.* **2012**, *12*, 6119−6125.
(43) Ohtake, A.; Mitsuishi, K. *J. Vac. Sci. Technol., B: Nanotechnol. Microelectron.: Mater., Process., Meas., Phenom.* **2011**, *29*, 031804.
(44) Paszuk, A.; Brückner, S.; Steidl, M.; Zhao, W.; Dobrich, A.; Supplie, O.; Kleinschmidt, P.; Prost, W.; Hannappel, T. *Appl. Phys. Lett.* **2015**, *106*, 231601.
(45) Gatos, H. C. *J. Appl. Phys.* **1961**, *32*, 1232−1234.
(46) Warekois, E. P.; Lavine, M. C.; Mariano, A. N.; Gatos, H. C. *J. Appl. Phys.* **1962**, *33*, 690−696.
(47) Ikejiri, K.; Ishizaka, F.; Tomioka, K.; Fukui, T. *Nano Lett.* **2012**, *12*, 4770−4774.
(48) Ikejiri, K.; Ishizaka, F.; Tomioka, K.; Fukui, T. *Nano Lett.* **2012**, *12*, 4770−4774.
(49) Poole, P. J.; Lefebvre, J.; Fraser, J. *Appl. Phys. Lett.* **2003**, *83*, 2055.
(50) Gao, Q.; Saxena, D.; Wang, F.; Fu, L.; Mokkapati, S.; Guo, Y.; Li, L.; Wong-Leung, J.; Caroff, P.; Tan, H. H.; Jagadish, C. Selective-Area Epitaxy of Pure Wurtzite In P Nano wires: High Quantum Efficiency and Room-Temperature Lasing. *Nano Lett.* **2014**, *14*, 5206−5211.
(51) Algra, R. E.; Verheijen, M. A.; Borgström, M. T.; Feiner, L.-F.; Immink, G.; Van Enckevort, W. J. P.; Vlieg, E.; Bakkers, E. P. A. M. *Nature* **2008**, *456*, 369−372.
(52) Dalacu, D.; Kam, A.; Guy Austing, D.; Wu, X.; Lapointe, J.; Aers, G. C.; Poole, P. J. Selective-area vapour-liquid-solid growth of In P nano wires. *Nanotechnology* **2009**, *20*, 395602.
(53) Calahorra, Y.; Greenberg, Y.; Cohen, S.; Ritter, D. Native-oxide-based selective area growth of In P nano wires via metal-organic molecular beam epitaxy mediated by surface diffusion. *Nanotechnology* **2012**, *23*, 245603.
(54) Bengoechea-Encabo, A.; Barbagini, F.; Fernandez-Garrido, S.; Grandal, J.; Ristic, J.; Sanchez-Garcia, M. A.; Calleja, E.; Jahn, U.; Luna; Trampert, A. Understanding the selective area growth of GaN nano columns by MBE using Ti nano masks. *J. Cryst. Growth* **2011**, *325*, 89−92.
(55) Fernández-Garrido, S.; Kong, X.; Gotschke, T.; Calarco, R.; Geelhaar, L.; Trampert, A.; Brandt, O. Spontaneous nucleation and growth of GaN nano wires: the fundamental role of crystal polarity. *Nano Lett.* **2012**, *12*, 6119−6125.
(56) Bertness, K. A.; Roshko, A.; Mansfield, L. M.; Harvey, T. E.; Sanford, N. A. Mechanism for spontaneous growth of GaN nano wires with molecular beam epitaxy. *J. Cryst. Growth* **2008**, *310*, 3154−3158.
(57) Schuster, F.; Furtmayr, F.; Zamani, R.; Magén, C.; Morante, J. R.; Arbiol, J.; Garrido, J. A.; Stutzmann, M. Self-assembled GaN nano wires on diamond. *Nano Lett.* **2012**, *12*, 2199−2204.
(58) Müßener, J.; Teubert, J.; Hille, P.; Schäfer, M.; Schörmann, J.; Dela Mata, M.; Arbiol, J.; Eickhoff, M. Probing the Internal Electric Field in GaN/Al GaN Nano wire Hetero structures. *Nano Lett.* **2014**, *14*, 5118−5122.
(59) Wang, X.; Che, S. B.; Ishitani, Y.; Yoshikawa, A. Growth of In-polar and N-polar In N nano columns on GaN templates by molecular beam epitaxy. *Phys. Status Solidi C* **2006**, *3*, 1561−1565.
(60) Stoica, T.; Meijers, R.; Calarco, R.; Richter, T.; Lüth, H. MBE growth optimization of In N nano wires. *J. Cryst. Growth* **2006**, *290*, 241−247.
(61) Chang, Y.-L.; Li, F.; Fatehi, A.; Mi, Z. Molecular beam epitaxial growth and characterization of non-tapered In N nano wires on Si(111). *Nanotechnology* **2009**, *20*, 345203.
(62) Baxter, J. B.; Wu, F.; Aydil, E. S. Growth mechanism and characterization of zinc oxide hexagonal columns. *Appl. Phys. Lett.* **2003**, *83*, 3797.
(63) Sallet, V.; Sartel, C.; Vilar, C.; Lusson, A.; Galtier, P. Oppositecrystalpolaritiesobservedinspontaneousandvapour-liquid-solidgrown Zn O nano wires. *Appl. Phys. Lett.* **2013**, *102*, 182103.
(64) Utama, M. I. B.; Belarre, F. J.; Magen, C.; Peng, B.; Arbiol, J.; Xiong, Q. In commen suratevander Waals Epitaxy of Nano wire Arrays: A Case Study with Zn O on Muscovite Mica Substrates. *Nano Lett.* **2012**, *12*, 2146−2152.
(65) Guillemin, S.; Rapenne, L.; Roussel, H.; Sarigiannidou, E.; Brémond, G.; Consonni, V. Formation Mechanisms of ZnO Nano wires: The Crucial Role of Crystal Orientation and Polarity. *J. Phys. Chem. C* **2013**, *117*, 20738−20745.
(66) Sun, Y.; Cherns, D.; Doherty, R. P.; Warren, J. L.; Heard, P. J. Reduction of threading dislocations in ZnO/(0001) sapphire film hetero structure by epitaxial lateral over growth of nano rods. *J. Appl. Phys.* **2008**, *104*, 023533.
(67) Nicholls, D. P.; Vincent, R.; Cherns, D.; Sun, Y.; Ashfold, M. N. R. Polaritydeterminationofzincoxidenanorodsbydefocusedconvergent-beamelectrondiffraction. *Philos. Mag. Lett.* **2007**, *87*, 417−421.
(68) Scrymgeour, D. A.; Sounart, T. L.; Simmons, N. C.; Hsu, J. W. P. Polarityandpiezoelectricresponseofsolutiongrownzincoxidenanocrystalsonsilver. *J. Appl. Phys.* **2007**, *101*, 014316.
(69) Perillat-Merceroz, G.; Thierry, R.; Jouneau, P.-H.; Ferret, P.; Feuillet, G. Compared growth mechanisms of Zn-polar ZnO nano wires on O-polar ZnO and on sapphire. *Nanotechnology* **2012**, *23*, 125702.

DOI: 10.1021/acs.nanolett.9b00459
Nano Lett. XXXX, XXX, XXX−XXX

(70) Consonni, V.; Sarigiannidou, E.; Appert, E.; Bocheux, A.; Guillemin, S.; et al. Selective Area Growth of Well-Ordered ZnO Nano wire Arrays with Controllable Polarity. *ACS Nano* **2014**, *8*, 4761−4770.
(71) Jasinski, J.; Zhang, D.; Parra, J.; Katkanant, V.; Leppert, V. J. Application of channeling-enhanced electron energy-loss spectroscopy for polarity determination in ZnO nano pillars. *Appl. Phys. Lett.* **2008**, *92*, 093104.
(72) Guillemin, S.; Rapenne, L.; Roussel, H.; Sarigiannidou, E.; Brémond, G.; Consonni, V. Formation Mechanisms of ZnO Nano wires: The Crucial Role of Crystal Orientation and Polarity. *J. Phys. Chem. C* **2013**, *117*, 20738−20745.
(73) Güniat, L.; Caroff, P.; Fontcuberta i Morral, A. *Chem. Rev.* **2019**, DOI: 10.1021/acs.chemrev.8b00649.
(74) Dalacu, D.; Kam, A.; Guy Austing, D.; Wu, X.; Lapointe, J.; Aers, G. C.; Poole, P. J. *Nanotechnology* **2009**, *20*, 395602.
(75) Calahorra, Y.; Greenberg, Y.; Cohen, S.; Ritter, D. *Nanotechnology* **2012**, *23*, 245603.
(76) Perillat-Merceroz, G.; Thierry, R.; Jouneau, P.-H.; Ferret, P.; Feuillet, G. Compared growth mechanisms of Zn-polar ZnO nano wires on O-polar ZnO and on sapphire. *Nanotechnology* **2012**, *23*, 125702.
(77) Schuster, F.; Laumer, B.; Zamani, R.; Arbiol, J.; Stutzmann, M.; et al. *ACS Nano* **2014**, *8*, 4376−4384.
(78) Poole, P. J.; Lefebvre, J.; Fraser, J. Spatially controlled, nano particle-free growth of In P nano wires. *Appl. Phys. Lett.* **2003**, *83*, 2055.
(79) Sallet, V.; Sartel, C.; Vilar, C.; Lusson, A.; Galtier, P. Oppositecrystalpolaritiesobservedinspontaneousandvapour-liquid-solidgrown ZnO nano wires. *Appl. Phys. Lett.* **2013**, *102*, 182103.
(80) Urban, A.; Malindretos, J.; Klein-Wiele, J.-H.; Simon, P.; Rizzi, A. *New J. Phys.* **2014**, *16*, 019501.
(81) Schuster, F.; Furtmayr, F.; Zamani, R.; Magén, C.; Morante, J. R.; Arbiol, J.; Garrido, J. A.; Stutzmann, M. *Nano Lett.* **2012**, *12*, 2199−2204.
(82) Schuster, F.; Weiszer, S.; Hetzl, M.; Winnerl, A.; Garrido, J. A.; Stutzmann, M. *J. Appl. Phys.* **2014**, *116*, 054301.
(83) Furtmayr, F.; Teubert, J.; Becker, P.; Conesa-Boj, S.; Morante, J. R.; Chernikov, A.; Schäfer, S.; Chatterjee, S.; Arbiol, J.; Eickhoff, M. Carrier confinement in GaN/*Alx Ga*1-*xN* nano wire hetero structures ($0<x \leq 1$). *Phys. Rev. B: Condens. Matter Mater. Phys.* **2011**, *84*, 205303.
(84) Cherns, D.; Meshi, L.; Griffiths, I.; Khongphetsak, S.; Novikov, S. V.; Farley, N.; Campion, R. P.; Foxon, C. T. Defect reduction in GaN/(0001)sapphire films grown by molecular beam epitaxy using nano column intermediate layers. *Appl. Phys. Lett.* **2008**, *92*, 121902.
(85) Alloing, B.; Vézian, S.; Tottereau, O.; Vennégùes, P.; Beraudo, E.; Zuniga-Pérez, J.; et al. On the polarity of GaN micro-and nano wires epitaxially grown on sapphire (0001) and Si (111) substrates by metal organic vapour phase epitaxy and ammonia-molecular beam epitaxy. *Appl. Phys. Lett.* **2011**, *98*, 011914.
(86) Brubaker, M. D.; Levin, I.; Davydov, A. V.; Rourke, D. M.; Sanford, N. A.; Bright, V. M.; Bertness, K. A. Effect of AlN buffer layer properties on the morphology and polarity of GaN nano wires grown by molecular beam epitaxy. *J. Appl. Phys.* **2011**, *110*, 053506.
(87) Lin, Y. T.; Yeh, T. W.; Nakajima, Y.; Dapkus, P. D. Catalyst-free GaN nano rods synthesized by selective area growth. *Adv. Funct. Mater.* **2014**, *24*, 3162−3171.
(88) Carnevale, S. D.; Kent, T. F.; Phillips, P. J.; Sarwar, A. T. M. G.; Selcu, C.; Klie, R. F.; Myers, R. C. Mixed Polarity in Polarization-Induced p-n Junction Nano wire Light-Emitting Diodes. *Nano Lett.* **2013**, *13*, 3029−3025.
(89) Carnevale, S. D.; Kent, T. F.; Phillips, P. J.; Mills, M. J.; Rajan, S.; Myers, R. C. Polarization-induced pn-diodes in wide band gap nano wires with ultra violet electroluminescence. *Nano Lett.* **2012**, *12*, 915−920.
(90) Kong, X.; Ristić, J.; Sanchez-Garcia, M. A.; Calleja, E.; Trampert, A. Polarity determination by electron energy-loss spectroscopy: application to ultra-smal lIII-nitride semiconductor nano columns. *Nanotechnology* **2011**, *22*, 415701.
(91) Hestroffer, K.; Leclere, C.; Bougerol, C.; Renevier, H.; Daudin, B. Polarity of GaN nano wires grown by plasma-assisted molecular beam epitaxy on Si (111). *Phys. Rev. B: Condens. Matter Mater. Phys.* **2011**, *84*, 245302.
(92) Den Hertog, M. I.; González-Posada, F.; Songmuang, R.; Rouviere, J. L.; Fournier, T.; Fernandez, B.; Monroy, E.; Hertog, M. I. D.; Gonza, F.; Songmuang, R.; Rouviere, J. L.; Fournier, T.; Fernandez, B. Correlation of polarity and crystal structure with optoelectronic and transport properties of GaN/AlN/GaN nano wire sensors. *Nano Lett.* **2012**, *12*, 5691−5696.
(93) Urban, A.; Malindretos, J.; Simon, P.; et al. Ga-polar GaN nano column arrays with semi polar faceted tips. *New J. Phys.* **2013**, *15*, 053045.
(94) Zúñiga-Pérez, J.; Consonni, V.; Lymperakis, L.; Kong, X.; Trampert, A.; Fernández-Garrido, S.; Brandt, O.; Renevier, H.; Keller, S.; Hestroffer, K.; Wagner, M. R.; Reparaz, J. S.; Akyol, F.; Rajan, S.; Rennesson, S.; Palacios, T.; Feuillet, G. *Appl. Phys. Rev.* **2016**, *3*, 041303.
(95) Tessarek, C.; Fladischer, S.; Dieker, C.; Sarau, G.; Hoffmann, B.; Bashouti, M.; Göbelt, M.; Heilmann, M.; Latzel, M.; Butzen, E.; Figge, S.; Gust, A.; Höflich, K.; Feichtner, T.; Büchele, M.; Schwarzburg, K.; Spiecker, E.; Christiansen, S. *Nano Lett.* **2016**, *16*, 3415−3425.
(96) Lee, S. H.; Minegishi, T.; Park, J. S.; Park, S. H.; Ha, J. S.; Lee, H. J.; Lee, H. J.; Ahn, S.; Kim, J.; Jeon, H.; Yao, T. Ordered arrays of ZnO nano rods grown on periodically polarity-inverted surfaces. *Nano Lett.* **2008**, *8*, 2419−2422.
(97) Park, J.; Kim, K. H.; Park, S. H.; Yoon, E.; Yao, T. Catalyst-free growth of vertically aligned ZnO nano structures arrays on periodically polarity-inverted substrate. *Appl. Phys. Express* **2010**, *3*, 105001.
(98) Park, J.; Yao, T. Position-controlled vertical arrays of single-crystalline ZnO nano wires on periodically polarity inverted templates. *J. Alloys Compd.* **2012**, *513*, 180−183.
(99) Consonni, V.; Sarigiannidou, E.; Appert, E.; Bocheux, A.; Guillemin, S.; et al. *ACS Nano* **2014**, *8*, 4761−4770.
(100) Utama, M. I. B.; Belarre, F. J.; Magen, C.; Peng, B.; Arbiol, J.; Xiong, Q. *Nano Lett.* **2012**, *12*, 2146−2152.
(101) Manna, L.; Scher, E. C.; Alivisatos, A. P. *J. Am. Chem. Soc.* **2000**, *122*, 12700−12706.
(102) Milliron, D. J.; Hughes, S. M.; Cui, Y.; Manna, L.; Li, J.; Wang, L.-W.; Alivisatos, A. P. Colloidal nano crystal hetero structures with linear and branched topology. *Nature* **2004**, *430*, 190−195.
(103) Deka, S.; Miszta, K.; Dorfs, D.; Genovese, A.; Bertoni, G.; Manna, L. Octa pod-shaped colloidal nano crystals of cadmium chalcogenides via "one-Pot" cation exchange and seeded growth. *Nano Lett.* **2010**, *10*, 3770−3776.
(104) Shiojiri, M.; Kaito, C. *J. Cryst. Growth* **1981**, *52*, 173−177.
(105) Zamani, R. R.; Ibáñez, M.; Luysberg, M.; García-Castelló, N.; Houben, L.; Prades, J. D.; Grillo, V.; Dunin-Borkowski, R. E.; Morante, J. R.; Cabot, A.; Arbiol, J. *ACS Nano* **2014**, *8*, 2290−2301.
(106) Wang, Z.; Kong, X.; Zuo, J. *Phys. Rev. Lett.* **2003**, *91*, 185502.
(107) Moore, D.; Wang, Z. L. *J. Mater. Chem.* **2006**, *16*, 3898−3905.
(108) Wang, Y.; Wang, G. Z.; Yau, M. Y.; To, C. Y.; Ng, D. H. L. *Chem. Phys. Lett.* **2005**, *407*, 510−515.
(109) Ma, D. D. D.; Lee, C. S.; Au, F. C. K.; Tong, S. Y.; Lee, S. T. *Science* **2003**, *299*, 1874−1877.
(110) Utama, M. I. B.; Dela Mata, M.; Zhang, Q.; Magen, C.; Arbiol, J.; Xiong, Q. *Cryst. Growth Des.* **2013**, *13*, 2590−2596.
(111) Cohen, D.; Mc Kernan, S.; Carter, C. *Microsc. Microanal.* **1999**, *5*, 173−186.
(112) Ramsdell, L. S. Studies on silicon carbide. *Am. Mineral.* **1947**, *32*, 64−82.
(113) Soler, J. M.; Artacho, E.; Gale, J. D.; Garcia, A.; Junquera, J.; Ordejon, P.; Sanchez Portal, D. *J. Phys.: Condens. Matter* **2002**, *14*, 2745−2779.

DOI: 10.1021/acs.nanolett.9b00459
Nano Lett. XXXX, XXX, XXX−XXX